Physics Insight and Performance Benefit in MHD and Energy Transport from Plasma Shaping Experiments in the TCV Tokamak

A. Pochelon, S. Brunner, Y. Camenen[1], S. Coda, J. Graves, A. Marinoni, An. Martynov, H. Reimerdes[2], O. Sauter, A. Scarabosio[3], S. Alberti, P. Angelino[4], R. Behn, A. Bortolon, A. Bottino[3], L. Curchod, K. Daouk, B.P. Duval, A. Fasoli, I. Furno, T.P. Goodman, M.A. Henderson, F. Hofmann, A. Karpushov, X. Lapillonne, J.B. Lister, Y. Martin, J-M. Moret, S. Medvedev[5], J.I. Paley, R.A. Pitts, F. Piras, L. Porte, H., F. Ryter[3], L. Sulmoni, A. Sushkov[6], L. Villard, M.Q. Tran, H. Weisen and the TCV Team

Ecole Polytechnique Fédérale de Lausanne (EPFL), Centre de Recherches en Physique des Plasmas, Association EURATOM-Confédération Suisse, CH-1015 Lausanne, Switzerland
[1]Centre for Fusion, Space and Astrophysics, Dept. of Physics, University of Warwick, UK
[2]General Atomics, San Diego, CA, US
[3]Max Planck Institut für Plasmaphysik (IPP), Garching bei München, Germany
[4]CEA-Cadarache, Association Euratom-CEA, Saint-Paul-Lez-Durance, France
[5]Keldysh Institute, Russian Academy of Sciences, Moscow, Russian Federation
[6]Institute of Nuclear Fusion, RRC "Kurchatov Institute", Moscow, Russian Federation
e-mail contact of main author: Antoine.Pochelon@epfl.ch

Abstract: The unique flexibility of TCV in plasma shaping has been exploited to address different aspects of tokamak physics, for which the plasma shape may play a role. This paper summarizes the experiments undertaken in the TCV tokamak ("Tokamak à Configuration Variable") over the last decade essentially in stability and transport. This paper enables a comprehensive and integrated view of the various specific effects of plasma shape observed. In each specific topic addressed, the relation between experimental results and theoretical predictions is stressed. Many of these topics are related to vital issues in ITER and to concept improvement in view of DEMO.

1. Introduction

Over the past decade, the TCV tokamak has produced world-leading physics results on diverse topics such as sawteeth, ELMs, ECH and ECCD, plasma control, MHD stability and eITB. A non-negligible proportion of these results have largely benefited from plasma shaping experiments. The TCV tokamak is indeed unique in the world fusion program in having the flexibility to produce plasmas with extreme shaping of the poloidal cross-section and up to 4.5MW of localized EC heating. This enables undertake specific studies over an unparalleled range of shapes, in limited and diverted configurations, including a broad range of elongations, with also triangularities ranging from positive to negative.
The characterization of the various effects of shaping serves at least two purposes: 1) it provides challenging tests for transport and stability theories, being thus a proficient tool for model validation, and 2) it is crucial for the design of future devices beyond ITER, since plasma shape has a strong influence on confinement, MHD stability and performance. For instance, it is well known that increasing the elongation increases the maximum plasma current as $(1+\kappa^2)/2$, without increasing the magnetic field. This affects three basic performance parameters, namely energy confinement [1], pressure [2] and density [3] limits, all scaling linearly with the plasma current. More recently, it has been shown that triangularity also strongly affects performance: energy confinement in H-mode [4] increases with respect to increasing triangularity, due to the pedestal, whereas core confinement is improved with increasing negative triangularity in L-mode [5,6], both by a factor of two, typically.

The TCV tokamak has been designed to produce a large variety of plasma shapes without requiring hardware modifications [7]. The basic TCV parameters are: major radius

R_0 = 0.88 m, minor radius a < 0.255 m (with an aspect ratio R/a ~ 2.9-3.5 close to ITER (6.2/2 = 3.1)), magnetic field B_T < 1.54 T, and plasma current $I_p \leq$ 1MA. The interior wall is totally covered with carbon tiles, and the vacuum vessel, of 2.9 elongation, allows the development of different divertor configurations. Plasma edge triangularity -0.8 < δ < 1 and elongation 0.9 < κ < 2.8 have been achieved [8]. Squarness can be used, e.g. to improve vertical stability. There are 16 independently driven shaping coils located between the vacuum vessel and the toroidal field coils and two additional poloidal field coils mounted inside the vacuum vessel for the control of plasmas with very high vertical instability growth rates. TCV has a plasma control system based on analog-digital hybrid technology [9], which is gradually changing to fully digital [10].

Electron Cyclotron (EC) waves offer localized power deposition and coupling independent of plasma-launcher distance. The TCV EC system is composed of six 2nd harmonic X2 gyrotrons with low field side (LFS) launchers (3MW, 82.7GHz, $n_{e\ cutoff\ X2} = 4.3\ 10^{19} m^{-3}$) [11] and three 3rd harmonic X3 gyrotrons with top launch (1.5MW, 118GHz, $n_{e\ cutoff\ X3} = 11.5\ 10^{19} m^{-3}$) [12, 13]. All launchers have two degrees of freedom and can be steered in real time. This gives TCV a flexible Electron Cyclotron (EC) system matching to its flexible plasma shaping capabilities. A high degree of automation, integration and flexibility in the experimental programme [14], allows TCV to explore a large spectrum of tokamak physics in different collisionality and confinement regimes, including low ITER-like collisionality.

3. q=1 MHD stability

Sawteeth, or q=1 relaxations, by abruptly flattening the core profiles, play a major role in redistributing the central pressure, heat, particles (thermal and energetic), impurity, momentum and current, thus influencing transport, and in triggering the seed islands which can initiate NTMs (neo-classical tearing modes), thereby degrading central pressure and confinement. An expression for the position of the q=1 radius, ρ_1, has been derived in TCV from the measurement of the sawtooth inversion radius over a large range of plasma shapes, [15,16]:
$\rho_{inv} \approx 2 / (q_{eng} (\kappa_0 + 1/\kappa_0))$, with $q_{eng} \equiv 5\kappa^2 a/RI_p$, and κ_0 the central elongation. This expression is largely used in the design of experiments to maintain self-similar profiles in subsequent studies of the effects of shape.

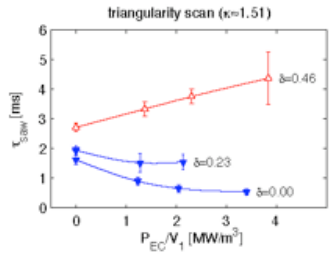

FIG. 1. Sawtooth period as a function of EC heating power density within the q=1 surface for different triangularities δ. Electron density and sawtooth inversion radius are kept constant.

Sawtooth period and amplitude were found to depend strongly on plasma shape, which was studied in systematic scans of plasma elongation and triangularity (-0.6<δ<0.5, 1.2<κ<2.8), keeping constant normalised q=1 radius ρ_1 [17, 18]. This results in:

- Long sawtooth period at high triangularity and intermediate elongation (0<δ<0.5, 1.2<κ<2.1) [17,18], and at high negative triangularity (down to δ=-0.6) [19].
- Short sawtooth period at low positive and slightly negative triangularity [17], or at high elongation (κ> ~2.4) [17].
- Transition to non-sawtoothing discharges at extreme elongations κ> ~2.4 [20].

With the addition of central EC power deposition inside the q=1 surface, the sawtooth period is found to either increase or decrease, depending on plasma shape, as shown in FIG.1. The sawtooth period increases with power at high triangularity δ>0.3 and decreases at low

triangularity. Similarly, the sawtooth period decreases with increasing elongations. The dependence on triangularity has been confirmed in JET [21, 22] and DIII-D [23].
The pressure profile build-up inside q=1 is determined by shape, as shown in FIG.2. The long sawtooth period which occurs for cases with high triangularity and low elongation allow the pressure profile inside q=1 to peaked strongly, limited by the sawtooth crash, thus by stability.

An analytic expansion of the ideal Mercier stability (necessary MHD) criterion [24] suggests that low triangularity and high elongation lead to lower ideal MHD central pressure limit at the q = 1 surface. In this triangularity range, ideal n=1 internal kink MHD calculations [17], using the KINX code [25], confirms that the internal kink mode is unstable for the lowest triangularity and highest elongation (and stable for the highest triangularity and lowest elongation). Thus, for plasma shapes where additional heating and, consequently, increased central pressure gradient shortens the sawtooth period, the low central pressure gradient limit achieved for certain shapes is consistent with ideal MHD predictions of internal kink stability. This is exemplified in the ohmic triangularity scan, see FIG.3 [19, 26].

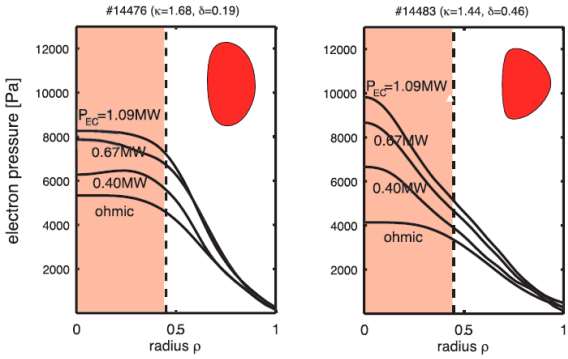

FIG. 2. The peaking of the pressure profile inside the q=1 surface, with the heating power deposited inside the q=1 surface, depends on plasma shape. The pressure profiles inside q=1 are peaked at high triangularity and low elongation, where Mercier stability improves (and where the internal kink is more stable).

The simulation of negative and positive triangularity experimental scans with the linear ideal MHD code KINX yields growth rates for the internal kink, which are lower for both positive and strongly negative triangularity, FIG.3b, in excellent correspondence with the experimental sawtooth period dependence. Such clear-cut results are understood physically by analytic expressions for the n=1 internal kink mode [26]. Calculations are faster using this analytical approach. Some of the shaping effects were shown to be identical to those obtained by the Mercier criterion.

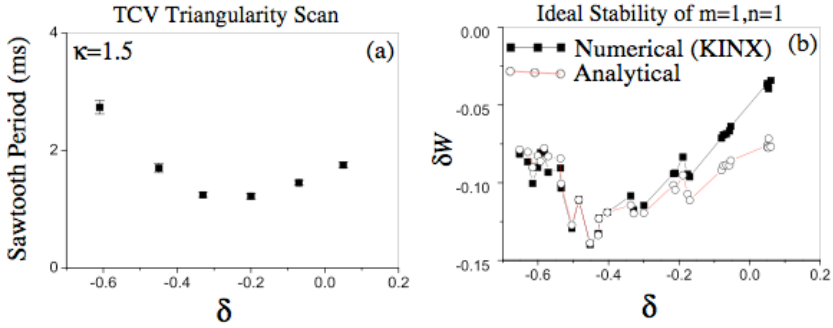

FIG. 3. Plot of (a) the sawtooth period in TCV over large negative to small positive triangularity for moderate elongation. The trend is very similar to (b) the ideal stability given by an analytic expression and by the KINX ideal MHD stability code.

Exploring elongations up to κ=2.8 in ohmic discharges revealed that for sufficiently high elongation, typically κ~2.5, there is a narrow threshold in internal inductance, around l_i~0.7, below which sawteeth abruptly disappear and are replaced by MHD mode activity [20, 27] without loss or shrinking of ρ_1. The threshold in l_i suggests the primary role of the current profile or shear. The pressure profile remains unchanged from sawtoothing to non-sawtoothing, remaining essentially flat inside ρ_{inv}~0.55–0.6, with the same clipping at ρ_1~ρ_{inv}, as shown e.g. by the electron temperature profile, FIG.4. Below l_i~0.7, sawteeth are replaced by continuous harmonic oscillations modes m/n= 1/1, 2/2 and 3/3 on q=1, FIG.5, with their

amplitudes $\xi_{m/n}$ only slowly decaying with m. The same phenomena can be observed at lower elongation ($2<\kappa<2.4$) using far-off axis EC heating to flatten the current profile and reach the inductance threshold [28-30]. Peaking the current profile by adding central (X3) EC heating reduces or suppresses the multi-harmonic modes, further underlining the correlation between a flat current profile or low shear s_1 at q=1 and the presence of harmonic modes [29, 28, 31].

Analytic and numerical ideal MHD calculations show that the internal kink mode becomes unstable, above a critical high κ, even with a flat pressure profile inside q=1. Hence instability occurs even though $\beta_{p,1}$=0. The sawtooth disappearance at extreme high elongation

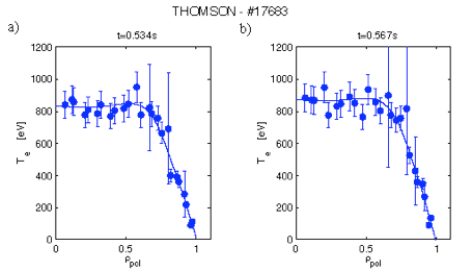

FIG. 4. Electron temperature profiles before (a) and after (b) the transition from a sawtoothing (κ=2.45) to a non-sawtoothing phase (κ=2.53).

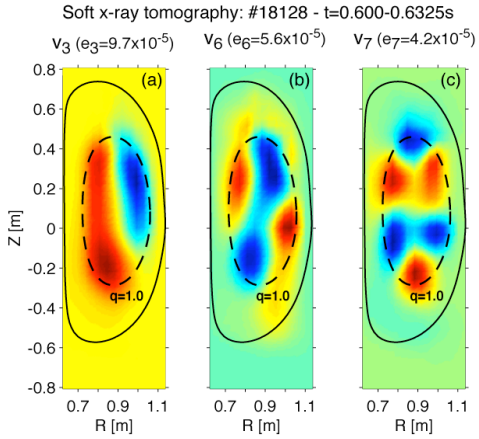

FIG. 5. First spatial eigenvectors of the tomographically reconstructed soft x-ray emissivity in a non-sawtoothing phase, showing (a) m=1 mode rotating at 5.1 kHz, (b) m=2 mode at 11.1 kHz and (c) m=3 structure at 17.1 kHz. A comparison with the frequencies of the toroidal mode component of magnetic measurements identifies the 1/1, 2/2 and 3/3 modes.

is well correlated with the ideal internal kink growth rate exceeding a finite positive threshold value, $\gamma_{ideal} > \omega_{*i}/2$ [20], thus requiring the ideal growth rate to overcome the stabilizing diamagnetic effects in order for the mode to become unstable [32]. Above this value, the internal kink is always unstable, in a state of continuous quasi-instability, regardless of pressure profile or current redistribution inside q=1.

It is suggested that the continuous MHD activity replacing sawteeth, the multi-harmonic modes located on q=1, are resistive modes destabilized by the proximity to the ideal MHD limit or ideal infernal modes generated in presence of a very flat central shear [33, 34]. This could explain the abrupt disappearance of finite amplitude sawteeth at high elongation [20].

Internal kink stability, tested on a very large range of plasma shapes, demonstrates the role of ideal MHD in explaining the essentials of the behaviour of sawteeth in TCV. These results illustrate the potential of using plasma shaping experiments to test and further improve modelling and theory, providing new insights into the nature of the sawtooth instability, together with practical formulas for integrated tokamak modelling.

3. Confinement and transport

An initial ohmic **confinement** study was undertaken in order to characterize the effect of plasma shape on electron energy confinement time τ_{Ee} in limited L-mode discharges [35,36]. Triangularity, elongation, density and edge safety factor were systematically varied over a broad parameters range ($1<\kappa<1.9$, $-0.4<\delta<0.7$, $2.4<q<4$, $5<\bar{n}_e<8\ 10^{19}$m^{-3}). For constant density and edge safety factor, the confinement time is found to decreases with triangularity and to increase with elongation, with saturation at high elongation ($2.2<\kappa<2.7$) [8].

Assuming diffusive heat transport, the flux surface averaged heat flux can be written as $Q_\alpha = -n_\alpha \chi_\alpha <|\nabla\rho|^2> (\partial T_\alpha / \partial\rho)$, with a metric term, $<|\nabla\rho|^2> \equiv f_g$, a geometric quantity related to the mean separation of flux surfaces directly resulting from plasma shape [35,36], the flux surface averaged gradient, and the radial heat diffusivity χ_e, which is a transport quantity related to collisional and turbulent processes. By changing triangularity from positive to negative values, the geometrical factor f_g does not vary substantially, in contrast to elongation, which strongly decreases f_g over the whole profile, see FIG.6. Thus, a large beneficial effect on confinement is expected from elongation, relying on geometrical effects alone. The impact of the f_g-profile on the confinement time can be calculated by comparing the confinement time of the real shaped plasma to the one of a circular plasma with the same diffusivity and heat flux profiles, $H_s = \tau_{Ee} / \tau_{Ee}^{circ}$, using ASTRA transport code. This ratio, known as the Shape Enhancement Factor (SEF) [35,36], is shown in FIG.7 versus elongation and triangularity [37]. It increases strongly with elongation, whereas it is almost independent of triangularity, see FIG.7 [37].

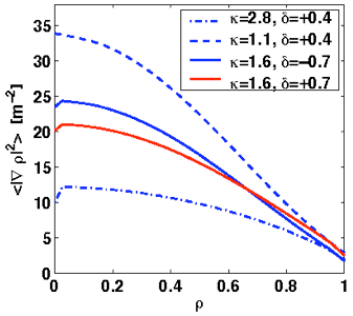

FIG. 6. Impact of κ and δ on the geometrical factor f_g profile. While the average flux surface compression is barely affected by large δchanges it is strongly modified by κ changes

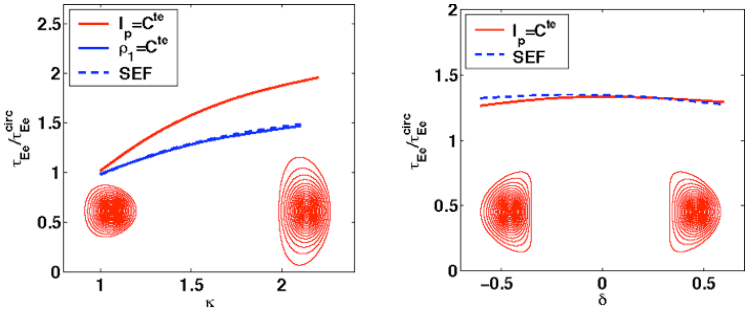

FIG. 7. Impact of elongation (a) and triangularity (b) on the confinement SEF maintaining constant current I_p (effect of geometrical factor f_g and of sawteeth) or constant q=1 surface radius ρ_1 (effect of geometrical factor only).

In theses ohmic studies, the measured τ_{Ee}, normalized by the SEF and the effect of power degradation, is close to constant, which demonstrates that for these plasmas, the effect of shape can be ascribed to the SEF, thus essentially a result of the metrics.
Furthermore, systematic confinement studies were undertaken using additional central EC heating at lower density, with power deposition inside a fixed ρ_1 ($1<\kappa<2.2$, $-0.65<\delta<0.5$, $n_{e0}\sim 2\ 10^{19} m^{-3}$) [38]. Over this extended triangularity range, a monotonic dependence on triangularity $\tau_{Ee} \sim (1+\delta)^{-0.35}$ was found, which was not symmetrical about δ=0. Thus the SEF contribution alone was not sufficient to describe the confinement variation, thus suggesting an additional dependence of χ_e on shape.

The role of plasma triangularity on heat **transport** was therefore investigated in plasma shaping experiments, combined with gradient variation experiments [5,6] to find out the relevant variables and decorrelate the experimental parameters. In the parameter range chosen for the investigation, it was found that the normalised temperature and density gradients have only a weak influence on heat transport. For fixed shape, χ_e was instead found to mainly scale with T_e, density and effective charge, these dependencies being combined into a dependence on the *effective collisionality* ν_{eff} [5], defined as the electron–ion collision frequency normalized to the electron curvature drift frequency, $\nu_{eff}=\nu_{ei}/\omega_{De} \sim 0.1\ R_0 n_e Z_{eff}/T_e^2$.
This finding allowed the investigation of the impact of triangularity on χ_e. The mid-radius electron heat diffusivity is plotted as a function of $1/\nu_{eff}$ in FIG.11, for positive and negative δ. The decrease in χ_e with increasing ν_{eff} is confirmed for each plasma shape and a clear

decrease in χ_e with decreasing plasma triangularity is obtained. For EC heated plasmas (full symbols), the electron heat transport decreases with increasing collisionality and decreasing triangularity. For ohmic plasmas (open symbols) with approximately the same electron density, the effective collisionality is higher and the triangularity effect on χ_e is barely observed. This underlines the strong impact of plasma collisionality on electron heat transport and possibly explains why the energy confinement improvement with decreasing plasma triangularity, observed in low collisionality EC heated plasmas [38,5], is not observed in high collisionality ohmic plasmas [35, 36].

The beneficial effect of negative triangularity is further illustrated by the comparison of two discharges at δ=±0.4. Both discharges have identical pressure profile, but the EC power for negative triangularity was half that for positive triangularity. As also shown in FIG.8, the heat diffusivity for the two cases follows in the heating power.

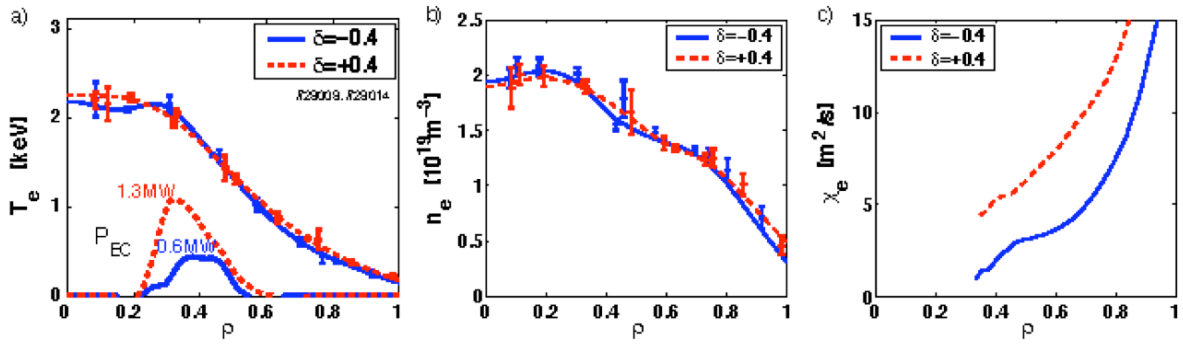

FIG 8. Comparison of two plasmas with different triangularities δ=±0.4, showing that for similar electron temperature (a) and electron density profile (b), the electron heat diffusivity (c) for δ=-0.4 is half of that for δ=+0.4. The EC power deposition location is shown in (a).

4. Effect of plasma triangularity on turbulent transport in gyrokinetic simulations

Gyrokinetic simulations are performed [39,40] on the basis of actual, self consistent MHD equilibrium reconstructions, focusing on the L-mode TCV discharges at δ=±0.4 for which the effect of plasma triangularity on heat transport has been evidenced [5,6]. Both GS2 (local) [41] and LORB5 (global) [42] **linear** simulations indicate that, for the experimental parameters, the dominant instability is a Trapped Electron Mode (TEM). In the $\delta < 0$ case, the growth rate of the most unstable mode is found 10% lower for each poloidal wave vector than in the $\delta > 0$ case. More importantly, the "transport effective" perpendicular wave vector of the mode, defined as the average along a field line of the local perpendicular wave vector $k_\perp$ weighted by the energy of the fluctuations [43], is found significantly higher at $\delta < 0$ than at $\delta > 0$ in the region of low poloidal wave vectors, i.e. $k_\theta \rho_i < 0.6$. These two effects result in a lower mixing length heat diffusivity, calculated as $\gamma / < k_\perp^2 >$, for the $\delta < 0$ case, and are explained as follows.

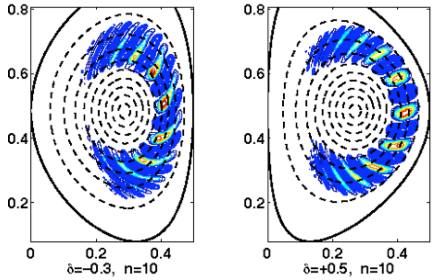

FIG. 9. Global linear gyro-kinetic simulations (LORB5) showing the impact of the plasma triangularity for (δ = -0.3 and δ = +0.5) on the TEM electrostatic potential cell orientation, for the n = 10 mode.

First, the local shear, s, is higher in the tips of the negative triangularity plasma compared to the positive triangularity case at the same LFS location. As the local perpendicular wave vector roughly scales as $k_\perp^2 = k_\theta^2(1 + s^2\theta^2)$, with θ the poloidal angle, the

increase in the local *shear* contributes to the increase of the effective $k_\perp$ at $\delta < 0$. The effect of the shear is also qualitatively observed in the global simulations, FIG.9 (poloidal cross-section shown), where the eddies of the electrostatic potential appear to be more tilted in the $\delta < 0$ case. Second, the change in the curvature and ∇B drifts modifies the toroidal precession drift of the trapped particles. As the TEM is intrinsically linked to the resonance with the toroidal precession drift, this modification can be expected to significantly affect the radial transport. The variation of the toroidal precession drift with the plasma triangularity is rather complex and depends on the pitch angle and energy of the trapped particles. For the particle energies at which most of the transport occurs, typically 2-3 T_e, the toroidal precession frequency is closer to the resonance condition at $\delta > 0$ than at $\delta < 0$ over most of the pitch angle domain.

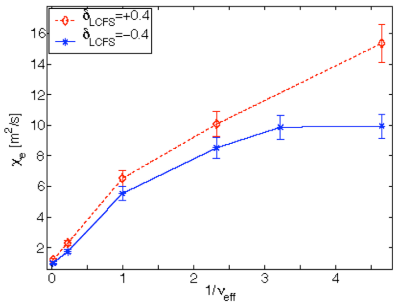

FIG 10. Effect of shape and collisionality on the non-linearly simulated electron heat diffusivity simulated with GS2 for δ=±0.4 (ρ=0.7) [39,40]

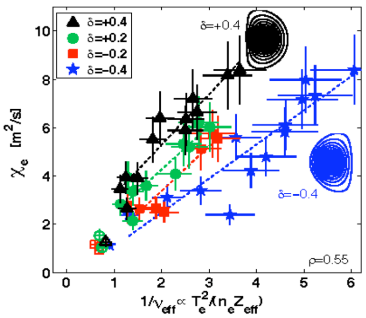

FIG 11. Corresponding experimental results (ρ=0.55) [6]

The **non-linear** simulations, all performed with the GS2 code, confirm the TEM nature of the most unstable mode, showing that trapped electrons carry the main part of the heat flux. The reduction of transport at negative triangularity, FIG. 10, is notably stronger than in the linear simulations and in fair quantitative agreement with the experimental results shown in FIG.11. The effect of the plasma collisionality is also investigated for comparison with the experimental results. As shown in FIG.12, the relative contribution of the trapped particles to the total heat flux decreases at high collisionality. By displacing the particles in phase space, collisions can indeed disrupt the resonance between the precession drift of the trapped electrons and the wave.

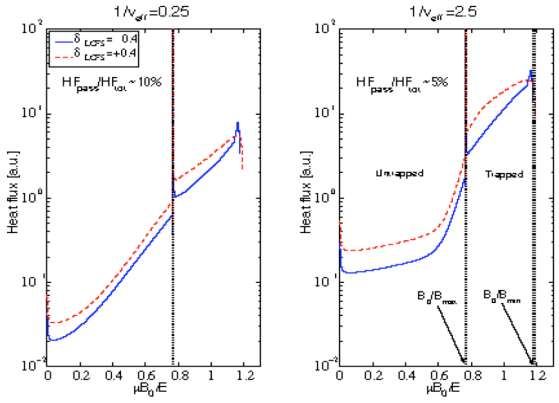

FIG 12. Heat Flux vs. pitch angle for two values of collisionality. At higher ν_{eff} the relative contribution from passing electrons to the total flux increases. Even though their contribution to the total flux is small, note how negative δ "stabilizes" also passing electrons (reduces the heat flux of passing electrons).

5. Conclusions and prospects

Optimizing performance, stability and confinement is vital in the search of an economical tokamak reactor. Plasma shaping is one of the important free operational parameters, strongly influencing plasma properties and performance, stability and transport as shown in this paper. Among the subjects not addressed in this brief paper, is the effect of shape on H-mode, extending plasma shapes to negative triangularities to study the influence on ELM stability and ELM regimes [44]. Negative triangularity H-modes can potentially lead to different

pedestal parameters, different ELM behaviour, and will allow the test of edge stability models over an extended triangularity range, and confinement studies aiming at better characterizing the role of edge and core confinement in H-mode. The ELM power load can also be mitigated in developing new advanced divertors, like the "snowflake divertor" [45], using a hexapole rather than dipole geometry to allow for a broader expansion of the flux surfaces. Different exotic and innovative shapes can be studied, like a doublet shape, with an X-point inside the plasma, a configuration that needs to be developed into a stable stationary configuration [46].

Acknowledgements. Many people have contributed to the material of this shape effects overview at various time of the progress of TCV and they are acknowledged here. This work was supported in part by the *Swiss National Science Foundation*.

References

[1] ITER Physics Basis, Nucl. Fusion **47** (2007) Chap. I, S1, eq. (3.1-1).
[2] TROYON, F., et al., Plasma Phys. Controlled Fusion **26** (1984) 209.
[3] GREENWALD, M., et al., Nucl. Fus. **28** (1988) 2199.
[4] STOBER, J., et al., Plasma Phys. Control. Fusion **42** (2000) A211.
[5] CAMENEN, Y., POCHELON, A., et al., Plasma Phys. Control. Fusion **47** (2005) 1971.
[6] CAMENEN, Y., POCHELON, A., et al., Nucl. Fusion **47** (2007) 510.
[7] HOFMANN, F., et al., Plasma Phys. Control. Fusion **36** (1994) B277.
[8] HOFMANN, F., et al., Plasma Phys. Control. Fusion **43** (2001) A161.
[9] LISTER, J.B., HOFMANN, F., MORET, J-M., et al., Fusion Science and Technol. **32** (1997) 321.
[10] PALEY, J., et al., this conference, EX/P6-16.
[11] GOODMAN, T.P., et al., Proc. 19th SOFT (Symp. on Fusion Technology), 1966, Lisbon, I, 565.
[12] HOGGE, J-Ph., et al., Nucl. Fus. **43** (2003) 1353.
[13] ALBERTI, S., et al., Journal of Physics: Conference Series **25** (2005) 210.
[14] GOODMAN, T.P., and the TCV Team, Nucl. Fus. **48** (2008) 054011.
[15] WEISEN H., et al., Phys. of Plasmas **6** (1998) 1.
[16] WEISEN, H., FURNO, I., et al., Nucl. Fusion **42** (2002) 136.
[17] REIMERDES, H., POCHELON, A., SAUTER, O., et. al., Plasma Phys. Control. Fusion **42** (2000) 629.
[18] REIMERDES, H., 2002 PhD Thesis No 2399, EPFL, Lausanne, Switzerland.
[19] MARTYNOV, An., GRAVES, J.P., and SAUTER, O., Plasma Phys. Control. Fusion **47** (2005) 1743.
[20] REIMERDES, H., et al., Plasma Phys. Control. Fusion **48** (2006) 1621.
[21] De VRIES, P.C., et al., 28th EPS Conf. on Contr. Fus. and Plasma Phys., ECA Vol. **25A** (2001) 1777.
[22] ANGIONI, C., POCHELON, A., et al., Plasma Phys. Control. Fusion **44** (2002) 205.
[23] LAZARUS, E.A., et al., Plasma Phys. Control. Fusion **48** (2006) L65.
[24] LüTJENS, H., BONDESON, A., and VLAD, G., Nucl. Fusion **32** (1992) 1625.
[25] DEGTYAREV, L., et al., Comput. Phys. Commun. **103** (1997) 10.
[26] GRAVES, J.P., et al., Plasma Phys. Control. Fusion **47** (2005) B121.
[27] POCHELON, A., HOFMANN, F., REIMERDES, H., et al., Nucl Fus. **41** (2001) 1663.
[28] SCARABOSIO, A., 2006 PhD Thesis No 3609, EPFL, Lausanne, Switzerland.
[29] CAMENEN, Y., HOFMANN, F., POCHELON, A., SCARABOSIO, A., et al., Nucl. Fusion **47** (2007) 586.
[30] SUSHKOV, A., CAMENEN, Y., POCHELON, A., et al., Rev. Sci. Instrum. **79** (2008) 023506.
[31] POCHELON, A., ARNOUX, G., CAMENEN, Y., SCARABOSIO, A. et al., IAEA FEC 2002, EX/P5-14.
[32] PORCELLI, F., BOUCHER, D., ROSENBLUTH, M.N., Plasma Phys. Control. Fusion **38** (1996) 2163.
[33] HASTIE, R.J., and HENDER, T.C., Nucl. Fusion **28** (1988) 585.
[34] WAHLBERG, C., and GRAVES, J., Physics of Plasmas **14** (2007) 110703.
[35] MORET, J.M., FRANKE, S., WEISEN, H., et al., Physical Review Letters **79** (1997) 2057.
[36] WEISEN, H., MORET, J-M., FRANKE S., FURNO I., et al., Nuclear Fusion **37** (1997) 1741.
[37] CAMENEN, Y., 2006 PhD Thesis No 3618, EPFL, Lausanne, Switzerland.
[38] POCHELON, A., GOODMAN, T.P., HENDERSON, M.A., et al., Nucl. Fusion **39** (1999) 1807.
[39] MARINONI, A., et al., 34th EPS Conf. on Plasma Phys., Warsaw, ECA Vol.**31F**, P1.067 (2007).
[40] MARINONI, A., et al., submitted to Plasma Phys. and Contr. Fusion, 2008.
[41] KOTSCHENREUTHER, M., REWOLDT, G., TANG, W.M., Comput. Phys. Commun. **88** (1995) 128.
[42] BOTTINO, A., et al., Phys. Plasmas **11** (2004) 198.
[43] JENKO, F., et al., Plasma Phys. and Contr. Fusion **47** (2005) B195.
[44] MEDVEDEV, S., et al., 35th EPS Conf. on Plasma Physics, Hersonissos, June 2008, Greece, P1.072.
[45] RYUTOV, D.D., et al., Physics of Plasmas **15**, (2008) 092501.
[46] HOFMANN, F., et al., Proc. 23rd EPS Conf. on Controlled Fusion and Plasma Physics, Kiev (1996).